MATERIALS FORUM VOLUME 32 - 2008
Edited by J.M. Cairney, S.P. Ringer and R. Wuhrer


# SEM INVESTIGATION OF HEAT TREATED HIGH-CHROMIUM CAST IRONS

**B. Hinckley [1], K.F. Dolman [1], R. Wuhrer [2], W. Yeung [3] and A. Ray [4]**

[1]Weir Minerals Australia Ltd, Locked Bag 51, Artarmon NSW 1570, Australia
[2]Microstructural Analysis Unit, [3] Department of Physics and Advanced Materials and [4] Chemistry Materials and Forensic Science, University of Technology, PO Box 123, Broadway, Sydney, NSW 2007, Australia

## ABSTRACT

Two high-chromium white cast irons, with compositions of Fe-25Cr-3.1C-2.0Mn-0.7Si and Fe-25Cr-5.2C-2.1Mn-0.4Si, were cast and subjected to various heat treatments. The microstructures were investigated using scanning electron microscopy and electron back-scattered diffraction techniques. The microstructure and properties were found to vary profoundly upon the increase in carbon content from 3 to 5%, changing from near-eutectic to hypereutectic and from a ferrous matrix of austenite partially transformed to martensite to one entirely transformed to pearlite. Age hardening followed by rapid cooling produced secondary carbides and a predominantly martensitic matrix in both alloys.

## 1. INTRODUCTION/BACKGROUND

White cast irons are widely used in applications requiring wear resistance. The unifying feature of all white cast irons is that their microstructures contain a significant proportion of a hard carbide phase. The reflective nature of these carbides on white iron fractures gives the characteristic "white" fracture appearance from which they originally derived their name [1]. More importantly, these hard carbides can provide excellent wear resistance [1-2].

A range of abrasion-resistant white cast irons are now specified in ISO 21988 [3] and also in ASTM A532 [4]. Abrasion-resistant white cast irons can be classified into three broad categories based on the level of chromium in the material:

1. Plain or unalloyed white cast irons and low alloy white cast irons (maximum of 2% chromium).
2. Nickel-chromium white cast irons, ie. Ni-Hard alloys (1.4-11% chromium).
3. High-chromium cast irons (>11% chromium).

This paper focuses on the high-chromium cast irons. The first high-chromium cast iron was patented by Becket in 1917 [5]. Becket's patented alloy covered the range of 25-30% chromium, 1.5-3% carbon and up to 3% silicon, although his most important alloy composition has been referred to as 27% chromium and 2.75% carbon [6]. High-chromium cast irons are classified in ISO 21988 as abrasion resistant cast irons that contain more than 11% chromium [3]. Typical compositions range from 11-40% chromium and 2.0-5.5% carbon, and they sometimes contain other alloying elements, such as molybdenum or nickel, to enhance specific properties. One distinguishing feature of the high-chromium cast irons is that the carbides are chromium rich; typically based on $M_7C_3$ [7], but also $M_{23}C_6$, depending on the chromium and carbon levels.

The ferrous matrix of high-chromium cast irons can be hardened by heat treatment at temperatures typically between 900-1050°C in order to develop maximum hardness and wear resistance. The heat treated microstructures typically consist of hard eutectic and secondary carbides in a matrix of martensite and retained austenite [8].

High-chromium white cast irons are primarily used as castings and hard-facing weld deposits in equipment requiring resistance to abrasive and erosive wear under low to moderate loading conditions. They are commonly used in the mining industry and in mineral and chemical processing plants in applications such as grinding mills, slurry pumps, chute liners and pipes.

High-chromium white cast irons owe their success to the presence of a significant proportion of chromium-rich carbide phase in their microstructures which imparts wear resistance for extended service life [9]. Wear-resistant high-chromium white irons are generally heat treated to develop maximum hardness via:

(a) precipitation of secondary carbides during ageing at elevated temperatures, and,
(b) destabilisation of austenite, which transforms to martensite upon cooling to room temperature.

The resultant microstructures typically consist of 20-50% by volume of chromium-rich carbides, with a hardness between 1200-1500 HV, in a hardened martensitic matrix with a hardness of approximately 700 HV. In many alloys, some austenite will be retained upon cooling to room temperature. Despite being wear resistant, high-chromium cast irons can be machined to high precision using cubic boron nitride (CBN) tool bits. The disadvantage of high-chromium white cast irons castings is that they can possess relatively low toughness (typically < 30 MPa$\sqrt{m}$) [9].

There are three fundamentally different microstructures that can be obtained in high-chromium cast irons by varying the carbon content. These three possible types are designated as follows:

- Hypoeutectic alloys
- Eutectic alloys
- Hypereutectic alloys

Eutectic alloys solidify at a single temperature and this occurs at a unique carbon level known as the eutectic composition. Eutectic alloys consist of a structure of eutectic carbide in a ferrous matrix. Hypoeutectic alloys are those that contain less carbon than the eutectic composition. In these alloys, a ferrous phase solidifies first in the form of dendrites and solidification occurs continuously over a range of temperatures down to the eutectic temperature. Hypereutectic alloys contain more carbon than the eutectic composition and primary carbide, normally hexagonal-shaped rods of $M_7C_3$, is the first phase to solidify.

High-chromium white irons undergo several solidification reactions and a number of different solid state transformation reactions on cooling to room temperature, and during reheating to elevated temperatures below the solidus. Consequently, a number of different phases form in high-chromium white irons that influence the mechanical properties and service life of the material. The following transformation reactions have been observed to occur in high chromium white cast irons:

- Primary austenite dendrites in hypoeutectic alloys.
- Primary $M_7C_3$ carbides in hypereutectic alloys.
- Eutectic carbide and austenite in hypoeutectic and hypereutectic alloys.
- Peritectic carbides in hypereutectic alloys.
- Secondary carbide precipitation during slow cooling after solidification or during ageing at elevated temperatures.
- Pearlite consisting of lamellar carbide and ferrite upon slow cooling.
- Decomposition of austenite to martensite on cooling.
- Transformation of tempered martensite to ferrite on reheating.
- Transformation of retained austenite to ferrite on reheating.
- Transformation of ferrite to austenite on reheating.
- Dissolution of pearlite to austenite on reheating.
- Dissolution of secondary carbides upon extreme reheating.

In this present study, microstructures of two high-chromium cast irons were examined in the as-cast, solution treated and age hardened conditions. Scanning electron microscopy (SEM) and electron back scattered diffraction (EBSD) were used to identify various transformation reaction products for these heat treated white cast irons. Thermal analysis and dilatometry assisted in explaining the structures obtained.

## 2. EXPERIMENTAL

### 2.1 Sample Preparation

The material used for this work was cast from a 25kg induction melting furnace into sand moulds to produce cast plates approximately 13mm thick. Two alloy compositions were studied. Chemical compositions are listed in Table 1.

The alloys are referred to throughout this report by their nominal compositions; ie. the 25-3 alloy and the 25-5 alloy, which represent 25%Cr with 3% carbon, and 25% chromium with 5% carbon, respectively.

Thermal analysis was conducted during the casting process. This was achieved by pouring approximately 2kg of molten metal into an insulative alumina fibre cup supported by silica sand. An R-type thermocouple (protected by a thin silica-glass sleeve) was inserted into this molten sample and connected to a datalogger to monitor the temperature of the sample throughout solidification and cooling to approximately 400°C.

Test coupons were sectioned from the cast plates using a water-cooled metallurgical cut-off saw. The as-cast surfaces were removed using a water-cooled swing grinder with a carborundum grinding cup. Small specimens were initially produced via cylindrical grinding followed by centreless grinding, and later by wire cutting to overcome difficulties with machining of these small brittle specimens. Disc specimens were sliced using a water-cooled, low-speed precision saw fitted with a diamond-coated metal blade.

One specimen from each experimental heat was examined in the as-cast condition. Further specimens were examined after being subjected to various heat treatments. Prior to heat treatment, the small specimens were encapsulated in silica-glass tubes under a partial pressure of argon in order to prevent oxidation, decarburisation and other elemental changes at the surface that can occur at the very high heat treatment temperatures. A schematic diagram of the silica-glass sealing apparatus used to encapsulate the specimens is shown in Figure 1.

**Table 1.** Experimental heat compositions – spectrographic results.

| Alloy | Chromium | Carbon | Manganese | Silicon | Nickel | Copper | Iron |
|---|---|---|---|---|---|---|---|
| 25-3 (Alloy 1) | 24.8 | 3.10 | 1.97 | 0.71 | 0.15 | 0.04 | Bal. |
| 25-5 (Alloy 2) | 24.9 | 5.18 | 2.05 | 0.44 | 0.15 | 0.04 | Bal. |

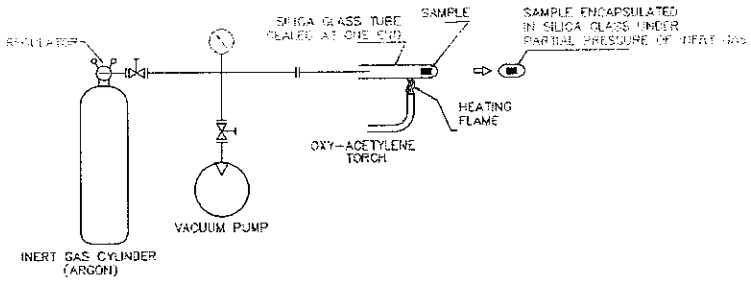


**Figure 1.** Schematic diagram of the silica-glass sealing apparatus.

The encapsulated samples were subjected to solution treatment at 1200°C for 1 hour and immediately water quenched to retain the high-temperature structure at room temperature and suppress any solid-state transformations during cooling. One sample was further subjected to a precipitation-hardening heat treatment at 950°C for 4 hours followed by water quenching. After heat treatment, the encapsulated samples exhibited a shiny unoxidised appearance (Figure 2), negligible weight change and metallographic examination of the transverse sections near the sample surface revealed no evidence of oxidation or decarburisation.

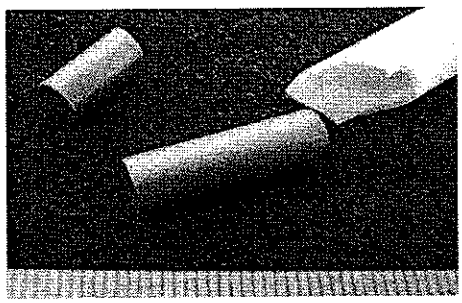

**Figure 2.** Encapsulated samples after heat treatment appeared unoxidised.

### 2.2 Characterisation of Samples

The specimens were prepared using standard metallographic techniques in a specially-designed sample holder to handle the small-sized specimens. Standard metallographic preparation techniques are not suitable for EBSD studies of white irons since mechanically induced surface distortion and stresses destroy the fine detail of the Kikuchi lines [10]. Electropolishing techniques were adopted for these white irons and this procedure yielded sharp EBSD patterns of the ferrous and carbide phases. The specimens were electropolished in a solution of 5% perchloric acid in ethanol using 39-42V at temperatures between 5°C to 25°C.

The specimens were examined under a Zeiss Supra 55VP field emission gun scanning electron microscope (FEGSEM) operated at 20kV accelerating voltage, 120um aperture, high current mode and using the back-scattered electron detector (BSE). Small specimens, nominally 6mm diameter x 2mm thick were prepared in the unmounted condition to facilitate electropolishing and to minimise charging and drift effects under the SEM. Conductive silver paint was applied around the entire circumference of the small samples to further minimise charging and drift. EBSD was performed at 20mm working distance using an HKL Technology EBSD system attached to the Zeiss Supra 55VP FEGSEM. The indexed solutions for the diffraction patterns were confirmed using independent software developed by Kogure [11].

Additional pin samples were taken from the experimental melts by inserting evacuated silica glass tubes into the open feeders on top of the castings. Dilatometry was performed using a Netzsch Model 402C Dilatometer on specimens taken from these pin samples. During dilatometry, the specimens were heated at a rate of 10 Kelvin per minute and cooled at a rate of 1.25 Kelvin per minute.

Hardness testing was conducted on a Vickers hardness tester using a 50kg indenter load. Ferromagnetism readings were performed using a Fisher Feritoscope calibrated using a set of standard non-magnetic film thickness gauges.

## 3. RESULTS AND DISCUSSION

### 3.1 Solidification of Alloys – Thermal Analysis Curves

Thermal analysis simply involves monitoring the temperature of the metal during cooling. As a material cools, if there are no phase transformations, the cooling rate follows a continuous exponential cooling curve. However, any changes to the structure upon cooling will normally produce a deviation from the ideal cooling curve since the change is either exothermic or

endothermic. Deviations from the ideal continuous cooling curve are observed and can be interpreted as phase changes. For example, the solidification reactions are exothermic so the liquidus and solidus temperatures can be readily identified as thermal arrest points. Another possible example in these alloys is the transformation of austenite to pearlite. The pearlitic transformation is also exothermic and can be seen as a thermal arrest on the cooling curve at temperatures of approximately 650-700°C.

### 3.1.1 25-3 Alloy (ie. Fe-25Cr-3.1C-2.0Mn-0.7Si)

At a first glance, the thermal analysis curve for the 25-3 alloy (Figures 3 and 4) appears to be typical of an eutectic alloy. Eutectic alloys show only a single thermal arrest during solidification. However, the curve for this alloy shows a very small initial peak at 1267°C, followed by a much larger arrest at 1265°C. The small initial peak corresponds to the first solidification reaction. It represents the liquidus temperature, which is the measurable exothermic reaction evolved due to the solidification of a small amount of primary phase according to the following equation:

Liquid → liquid + primary $M_7C_3$ carbide (s)

Therefore, Alloy 1 (25-3) is a near-eutectic alloy rather than a purely eutectic alloy. The small amount of heat generated at the liquidus temperature indicates that the volume fraction of primary phase is very small. An observation that is typical of near-eutectic alloys is that the liquidus temperature is very close to the solidus temperature; in this case the liquidus is only 2°C above the solidus. The larger arrest at 1265°C is due to the heat generated by the exothermic eutectic reaction according to the following equation:

Remaining liquid → eutectic (s)

Where:
eutectic(s) = eutectic austenite(s) + eutectic carbide(s)

The relatively large size of the thermal arrest at the solidus temperature indicates a relatively large proportion of the eutectic constituent. Solidification is complete at the end of the arrest at the solidus temperature. Upon further cooling down to around 400°C, no solid state transformations are evident from the thermal analysis curve for this alloy at the observed cooling rate.

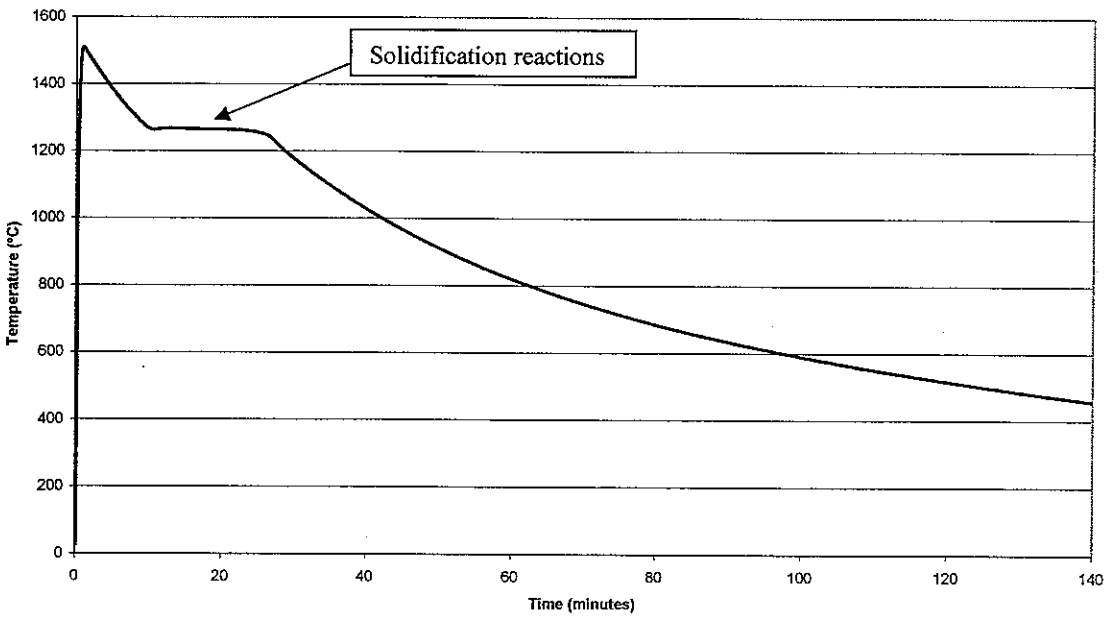


**Figure 3.** Thermal analysis cooling curve for the 25-3 alloy.

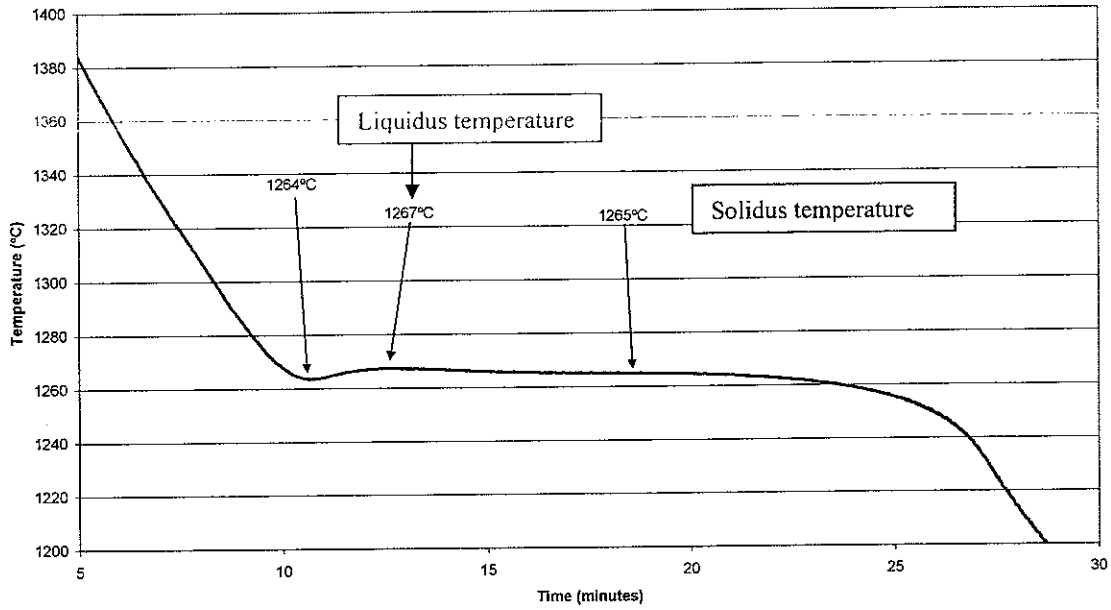


**Figure 4**. Solidification region of the thermal analysis curve for the 25-3 alloy.

### 3.1.2 25-5 Alloy (ie. Fe-25Cr-5.2C-2.1Mn-0.4Si)

The 25-5 alloy (Figure 5 and 6) is hypereutectic so it contains a primary carbide phase. Solidification of the primary phase begins at 1346°C according to the following reaction:

Liquid → liquid + primary carbide (s)

The liquidus temperature for Alloy 2 (25-5) is higher than the liquidus temperature for the near-eutectic Alloy 1 (25-3). Solidification of the remaining liquid occurs at the solidus temperature of 1239°C according to the equation:

Remaining liquid → eutectic (s)

Where:
eutectic (s) = austenite (s) + eutectic carbide (s).

It can be observed that the solidus temperature for the 25-5 alloy is lower than that of the 25-3 alloy. This indicates that, for Fe-25Cr-C alloys within the composition studied, the eutectic temperature decreases with increasing carbon content. In other words, the solidus line on the Fe-Cr-C phase diagram is not perfectly horizontal but slopes down slightly as the carbon increases.

Upon further cooling, the solid-state pearlite transformation begins at 680°C according to the following equation:

Austenite (s) → pearlite (s)

Where:
pearlite (s) = lamellar ferrite (s) + lamellar carbide (s).

Subsequent microstructural examination revealed that all of the austenite transformed to pearlite.

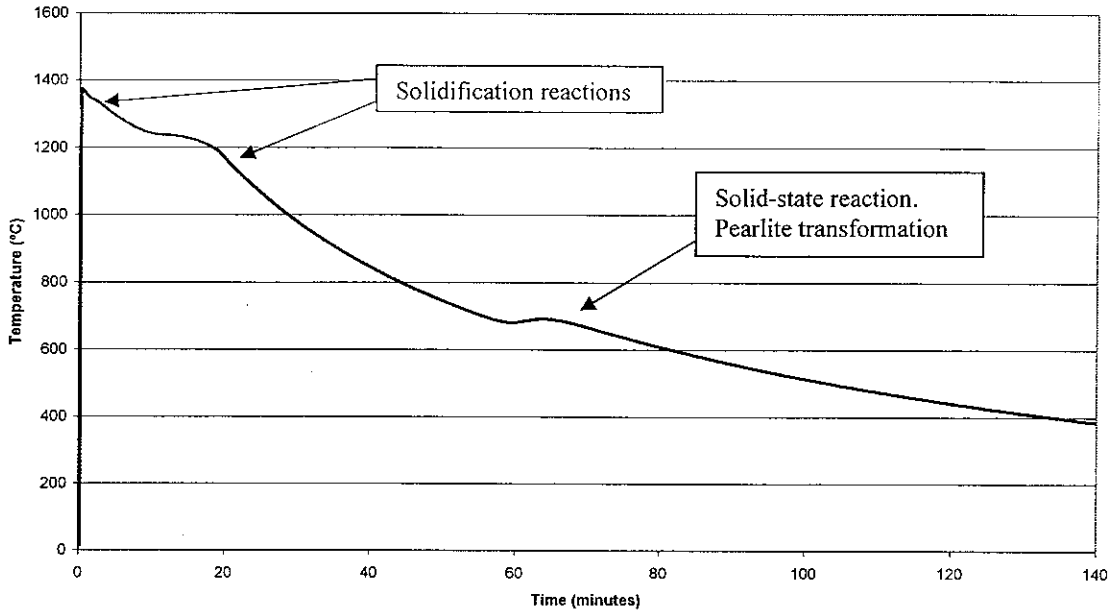


**Figure 5**. Thermal analysis cooling curve for the 25-5 alloy.

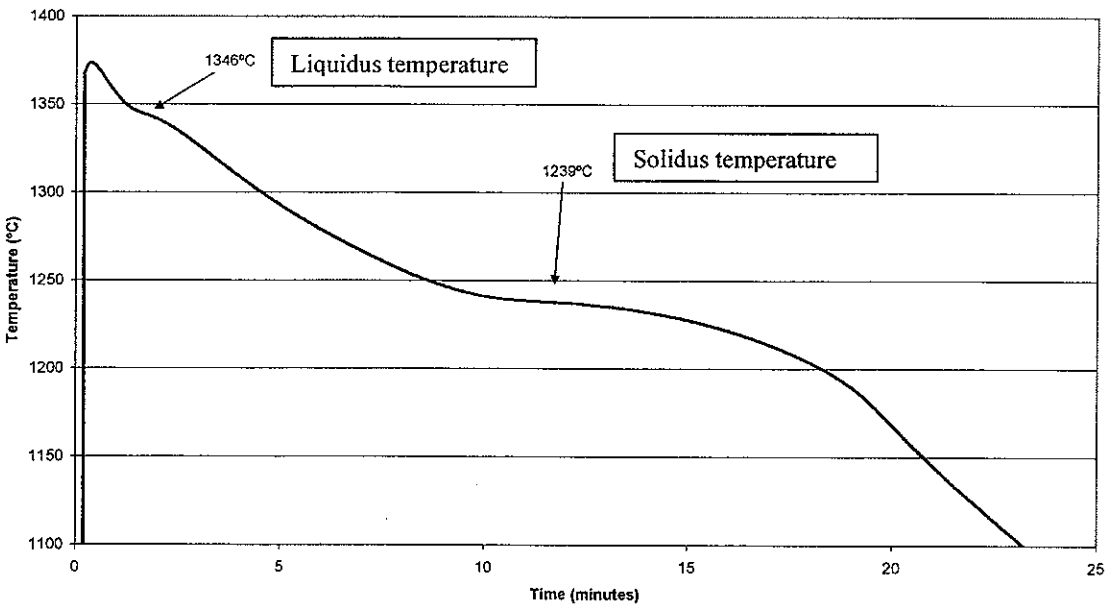


**Figure 6**. Solidification region of the thermal analysis curve for the 25-5 alloy.

Liquidus and solidus temperatures for 2kg metal samples were measured and shown in Table 2. Figure 7 shows graphically the measured liquidus and solidus temperatures for the two alloys and these curves constitute a small part of the phase diagram for the Fe-25Cr alloy system.

**Table 2.** Liquidus and solidus temperature measurements

| Alloy | Liquidus | Solidus | Pearlite Transformation |
|---|---|---|---|
| 25-3 (Alloy 1) | 1267°C | 1265°C | Not evident |
| 25-5 (Alloy 2) | 1346°C | 1239°C | Evident at 680-710°C |

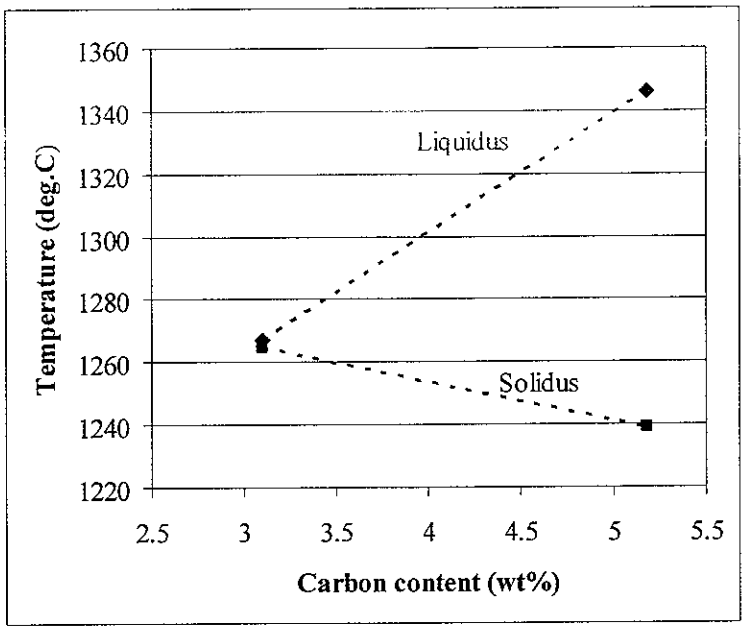


**Figure 7.** Measured liquidus & solidus temperatures for the two alloys.

### 3.2 Physical Properties

Vickers hardness test results and magnetic response are summarised in Table 3.

**Table 3:** Physical Property results for specimens

| Condition | Fe-25Cr-3C-2Mn-0.7Si | | Fe-25Cr-5C-2Mn-0.4Si | |
|---|---|---|---|---|
| | Vickers hardness ($HV_{50}$) | Magnetic response (%) | Vickers hardness ($HV_{50}$) | Magnetic response (%) |
| As cast | 616 | 12.1% | 629 | 30.5% |
| Solution treated at 1200°C for 2hrs | 538 | 1.4% | 585 | 1.1% |
| Aged at 950°C for 4hrs | 889 | 31.3% | 1030 | 21.9% |

### 3.3 Metallography & SEM Imaging

#### 3.3.1 25-3 Alloy (ie. Fe-25Cr-3.1C-2.0Mn-0.7Si)

In the as-cast condition, the 25-3 alloy consisted predominantly of eutectic carbides in a matrix of austenite with some transformation of the austenite to martensite, particularly adjacent to carbides (Figure 8). A small amount of primary carbides were also observed. Virtually no fine secondary carbides were evident.

In the solution treated and quenched condition, the wholly austenitic matrix exhibited relatively large grains with occasional annealing twins (Figure 9). The eutectic carbides appeared to be slightly rounded by the solution treatment. A small proportion of secondary carbides were observed, which indicates that the solution treatment temperature of 1200°C, being 65°C below the solidus temperature, or the holding time of one hour, was insufficient for the complete dissolution of all of the secondary carbides.

At 950°C, the ferrous matrix is supersaturated with respect to carbon and chromium. Therefore, during the aging heat treatment at 950°C for 4 hours, secondary carbides precipitate from the ferrous matrix (Figure 10). Consequently, the ferrous matrix becomes depleted with respect to carbon and chromium. The solute-depleted austenite becomes destabilised so that upon cooling the austenitic matrix transforms almost completely to martensite.

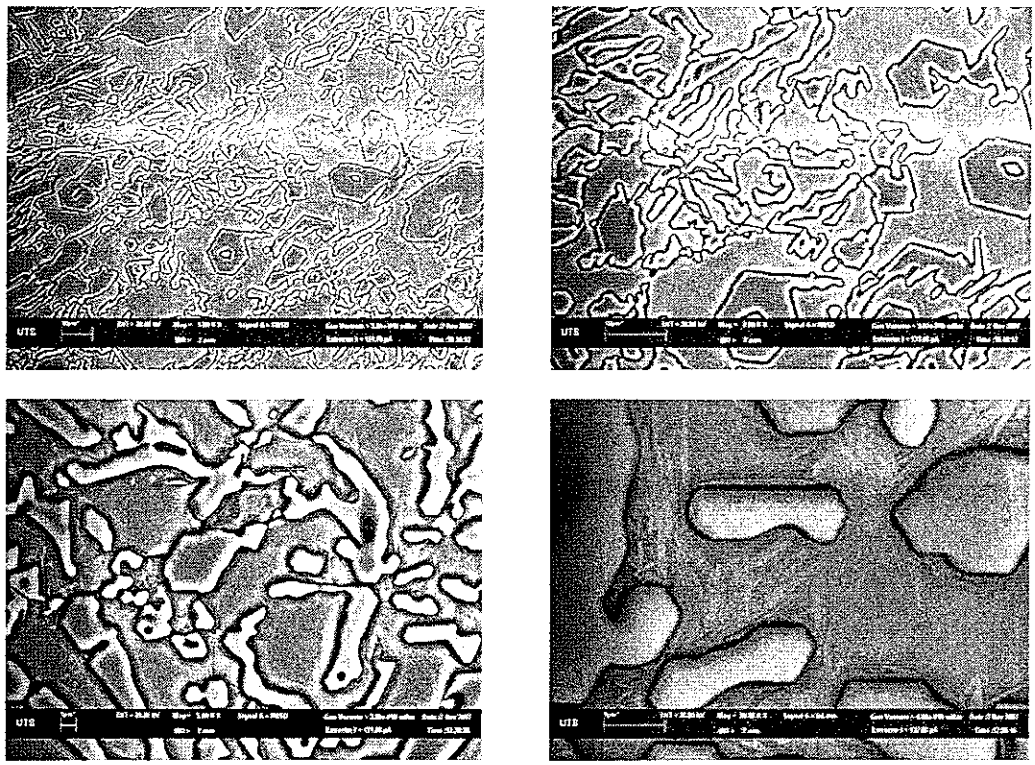

Figure 8. BSE images for the 25-3 alloy in the as-cast condition.

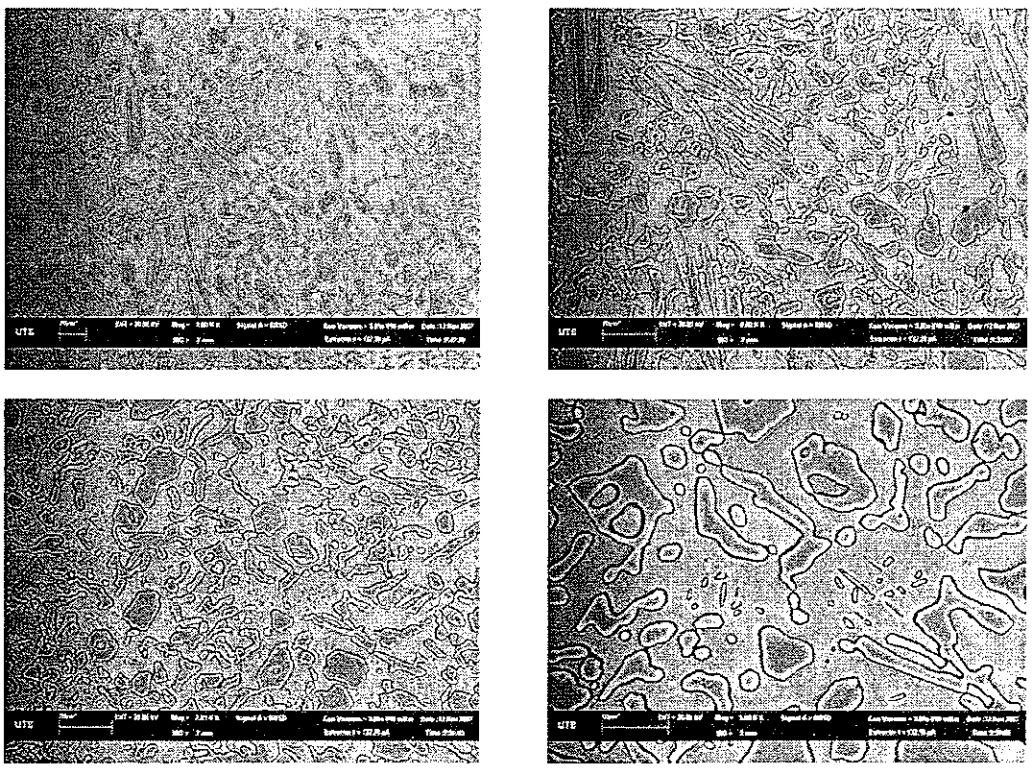

Figure 9. BSE images for the 25-3 alloy after solution treatment at 1200°C.

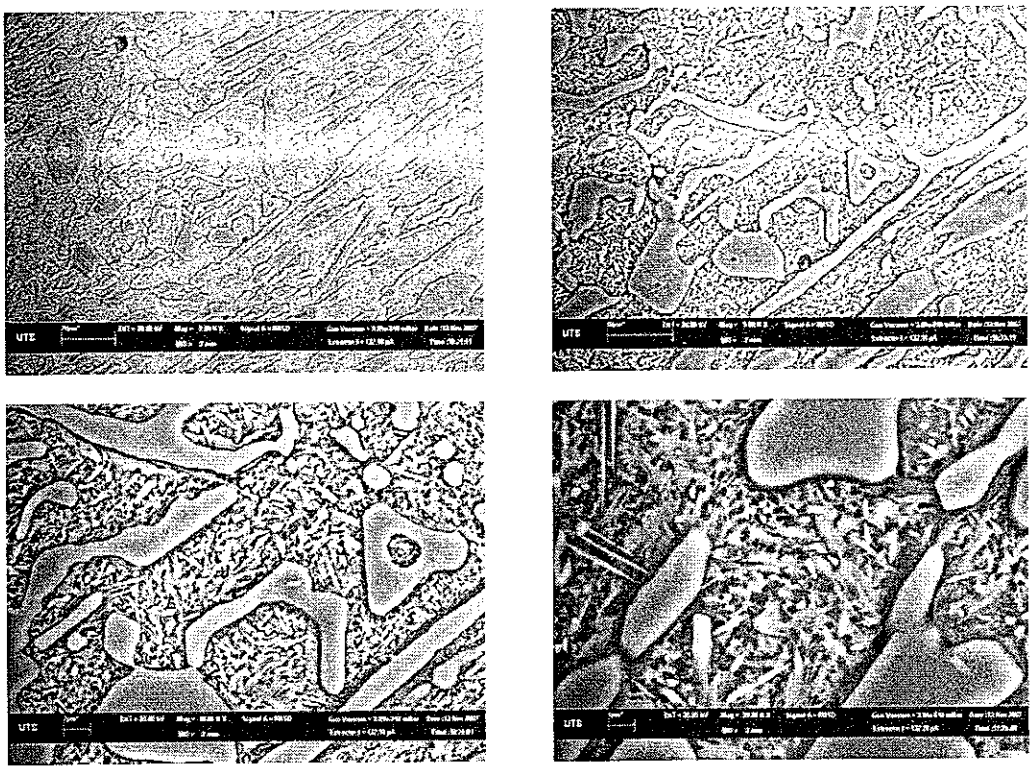

Figure 10. BSE images of the 25-3 alloy in the age-hardened condition.

### 3.3.2 25-5 Alloy (ie. Fe-25Cr-5.2C-2.1Mn-0.4Si)

In the as-cast condition, the 25-5 alloy consisted of primary carbides and eutectic carbides in a matrix fully transformed to pearlite (Figure 11).

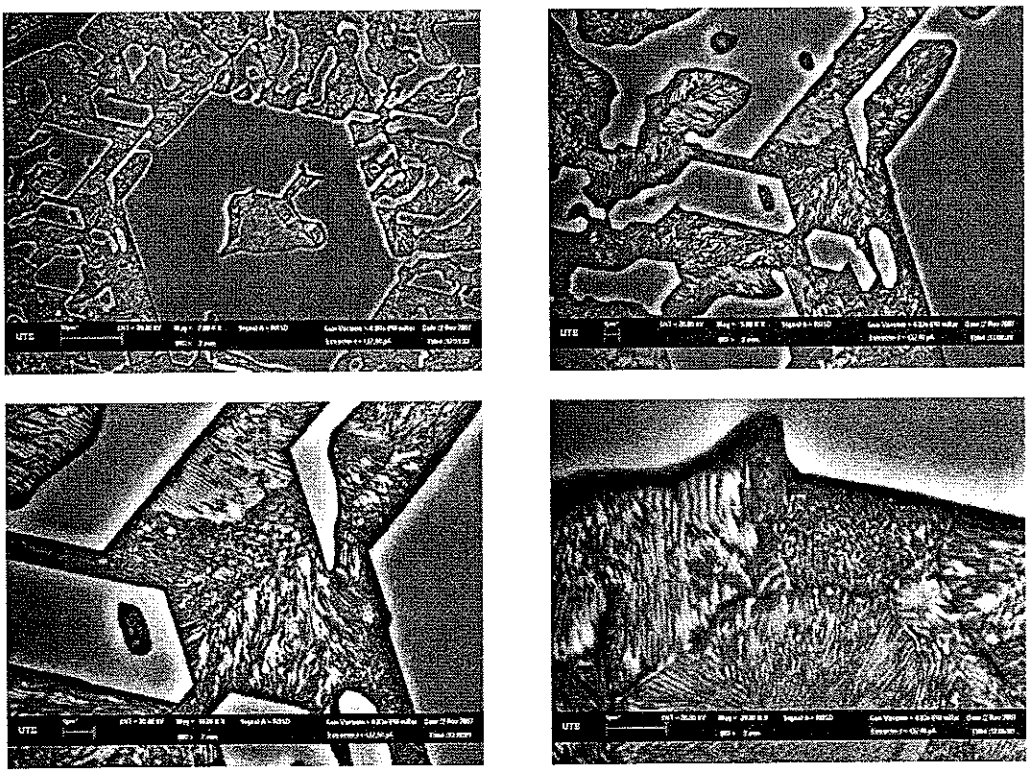

Figure 11. BSE images of the 25-5 alloy in the as-cast condition.

In the solution treated and quenched condition (Figure 12), the wholly austenitic matrix exhibited austenite grains with annealing twins evident in some grains. The eutectic carbides appeared to be slightly rounded by the solution treatment. Virtually no secondary carbides were evident, indicating that the solution treatment temperature of 1200°C, being only 39°C lower than the solidus temperature, and the one hour holding time, was sufficient for the complete dissolution of the fine secondary carbides, restoring the carbon and chromium concentrations in the matrix to their maximum levels.

Upon reheating to 950°C, the alloy matrix is now supersaturated with respect to carbon and chromium and during the aging heat treatment at 950°C for 4 hours secondary carbides precipitate from the ferrous matrix (Figure 13). Consequently, the ferrous matrix becomes depleted with respect to carbon and chromium. The solute depleted austenite becomes destabilised so that upon cooling the austenitic matrix transforms almost completely to martensite.

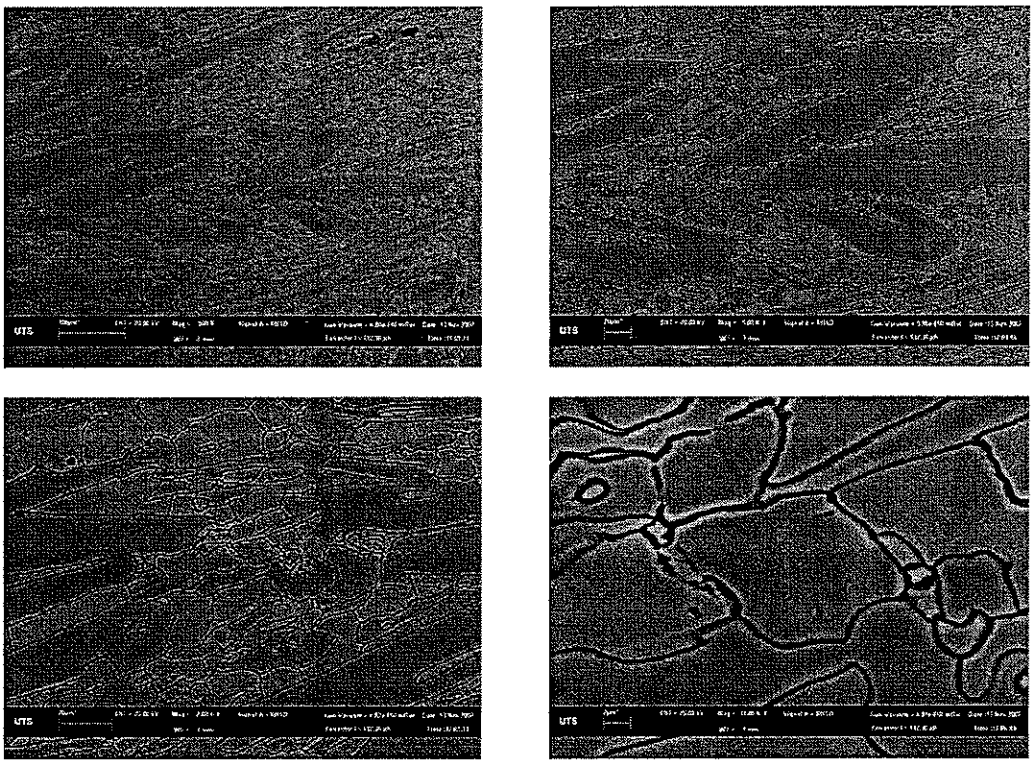

**Figure 12.** BSE images for the 25-5 alloy after solution treatment at 1200°C.

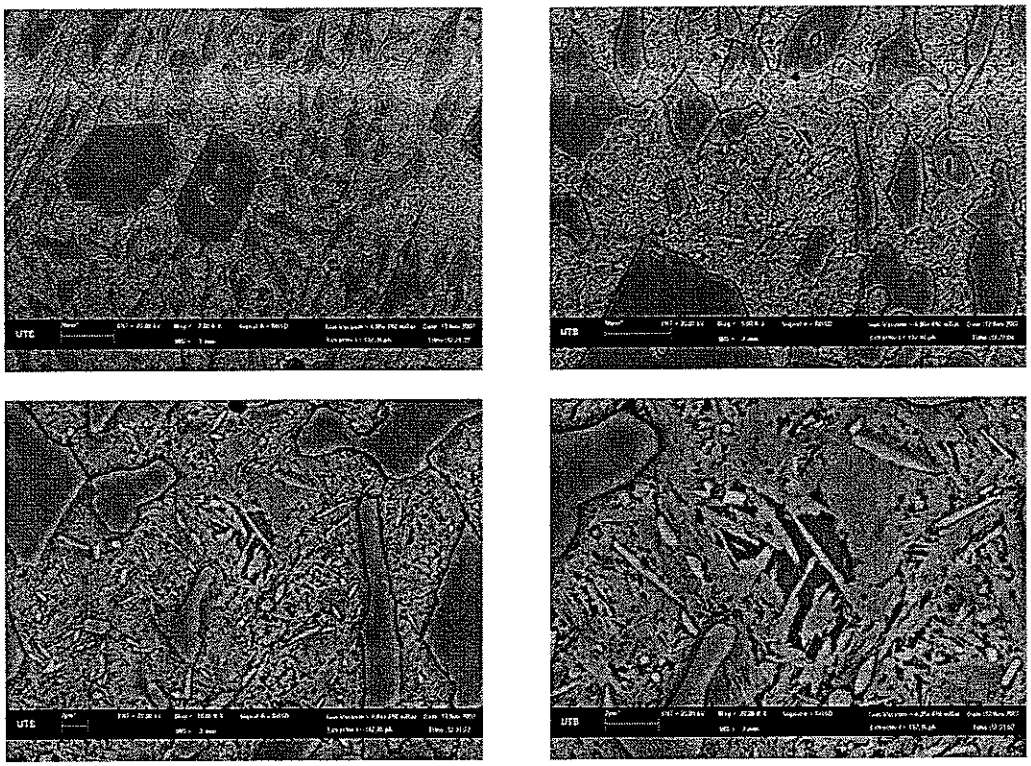

**Figure 13.** BSE images for the 25-5 alloy in the aged condition.

### 3.4 Electron Back Scattered Diffraction (EBSD)

EBSD investigations were carried out on both alloys in the solution treated and in the age-hardened conditions. These studies confirmed the crystal structures of the major phases in both alloys and the results are summarized in the Tables 4-7. The austenite grains in the solution treated samples were face centred cubic (space group 225). Upon age-hardening, the ferrous matrix transformed to martensite with some austenite being retained. Although martensite is body centred tetragonal, the tetragonality is only of the order of a few percent. EBSD studies are not effective for detecting this small degree of tetragonality. Consequently, martensite was identified in these EBSD studies as being body centred cubic.

A further limitation of EBSD was that the small amounts of retained austenite in the age-hardened samples did not yield idenitifiable Kikuchi patterns. This may be explained by the presence of martensite, which undergoes a volume expansion upon transformation. This volume expansion in the martensite phase may exert a stress on the retained austenite. This stress would strain the austenite crystal lattice and interfere with the development of Kikuchi lines during electron diffraction.

The primary and eutectic carbides were consistent with a hexagonal close packed structure with space group 186, although they were also similar to the orthorhombic structure with space group 62. Examples of the EBSD patterns for the 25-5 alloy are shown in Figures 14 and 15.

**Table 4.** EBSD results for the 25-3 alloy in the solution treated condition

| Phase | Space Group | Crystal Structure |
|---|---|---|
| Primary carbide | 186 | Hexagonal close packed (similar to orthorhombic SG62) |
| Eutectic carbide | 186 | Hexagonal close packed (similar to orthorhombic SG62) |
| Austenite | 225 | Face centred cubic |

**Table 5.** EBSD results for the 25-3 alloy in the age-hardened condition

| Phase | Space Group | Crystal Structure |
|---|---|---|
| Primary carbide | 186 | Hexagonal close packed |
| Eutectic carbide | 186 | Hexagonal close packed |
| Martensite | 229 | Body centred cubic |

**Table 6.** EBSD results for the 25-5 alloy in the solution treated condition

| Phase | Space Group | Crystal Structure |
|---|---|---|
| Primary carbide | 186 | Hexagonal close packed |
| Eutectic carbide | 186 | Hexagonal close packed (similar to orthorhombic SG62) |
| Austenite | 225 | Face centred cubic |

**Table 7.** EBSD results for the 25-5 alloy in the age-hardened condition

| Phase | Space Group | Crystal Structure |
|---|---|---|
| Primary carbide | 186 | Hexagonal close packed |
| Eutectic carbide | 186 | Hexagonal close packed |
| Martensite | 229 | Body centred cubic |
| Austenite | No result could be obtained | |

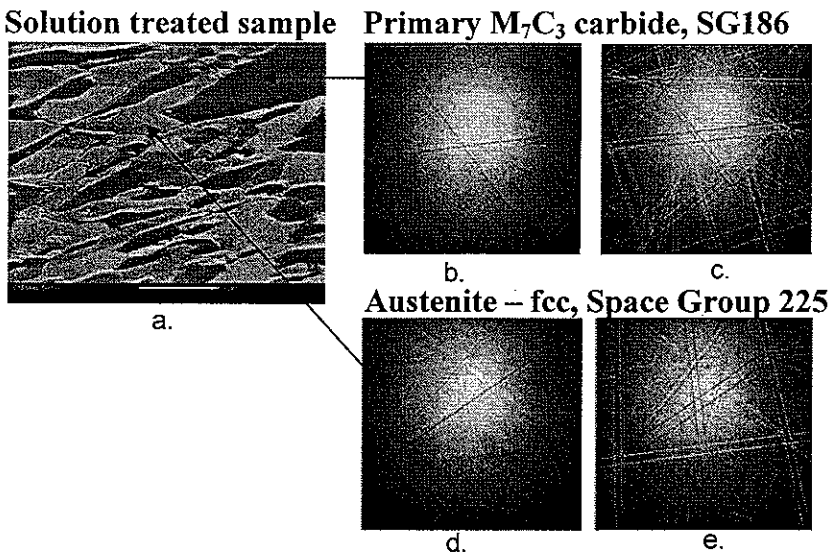


**Figure 14.** 25-5 Alloy solution treated sample; (a) microstructure, (b) EBSD patterns and (c) indexed EBSD result for primary carbide, (d) EBSD pattern and (e) indexed EBSD result for the austenite phase.

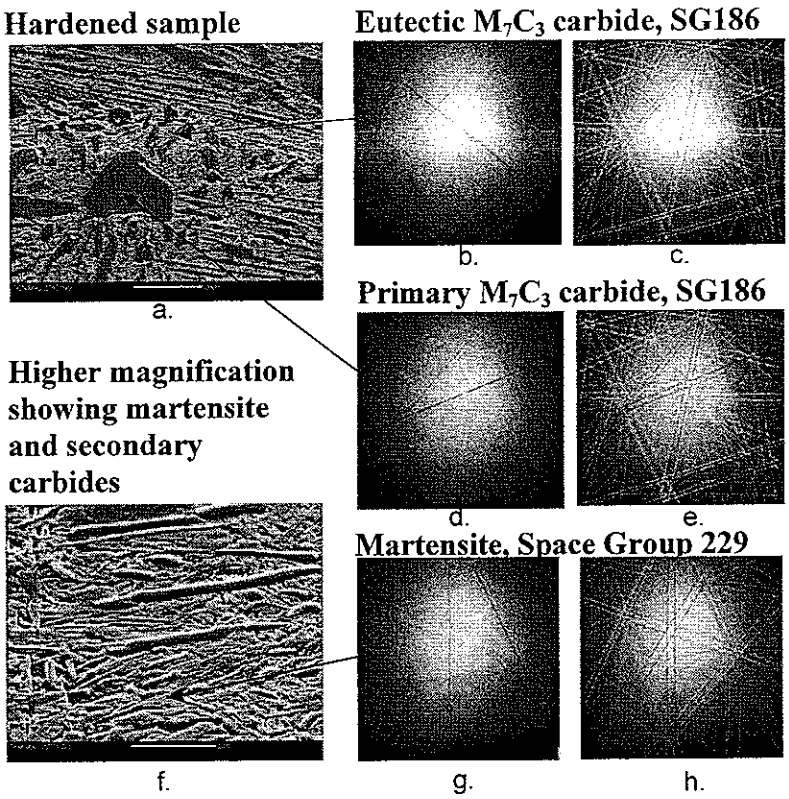


**Figure 15.** 25-5 Alloy age-hardened sample; (a) microstructure, (b) EBSD patterns and (c) indexed EBSD result for eutectic carbide, (d) EBSD pattern and (e) indexed EBSD result for the primary carbide, (f) microstructure showing martensite, (g) EBSD patterns and (h) indexed EBSD result for the martensitic matrix.

### 3.5 Dilatometry

Dilatometry is a metallurgical tool that is useful for determining coefficients of expansion and for detecting phase changes upon heating and cooling. Dilatometry involves subjecting a specimen to a thermal cycle while continuously measuring the length of the specimen. As the specimen is heated, it expands and this can be measured as an increase in length and the coefficient of thermal expansion versus temperature can be measured. In the same way, the thermal contraction can be measured as the specimen cools. Any phase changes that involve a change in the coefficient of expansion will show up as a change in slope, or inflection, in a plot of extension versus temperature. Any phase changes that involve a change in volume will appear as a dramatic change in the slope of the curve. All data results are shown in Tables 8 and 9, and Figures 16 to 19 for the two alloy types.

**Table 8.** Results from dilatometry to 1200°C for 2 hours.

| Alloy | Heating cycle | Cooling cycle | |
|---|---|---|---|
| | Austenite Transformation | Pearlite Transformation | Martensite Transformation |
| Fe-25Cr-3C | 810°C | 650°C | Ms = 375°C |
| Fe-25Cr-5C | 790°C | 680°C | No martensite |

**Table 9.** Results from dilatometry to 950°C for 4 hours.

| Alloy | Heating cycle | Cooling cycle | |
|---|---|---|---|
| | Austenite Transformation | Pearlite Transformation | Martensite Transformation |
| Fe-25Cr-3C | 805°C | 650°C | Ms = 385°C |
| Fe-25Cr-5C | 810°C | 680°C | No martensite |

Note: The martensite start temperature is denoted as Ms.

Dilatometer Curves for the 25-3 Alloy

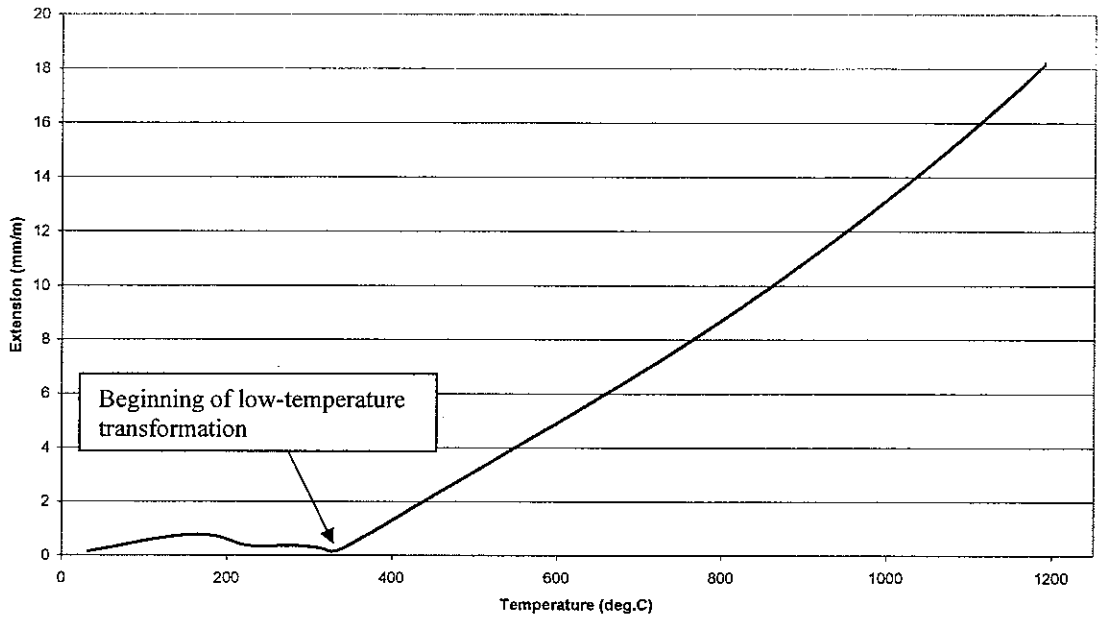


**Figure 16.** Dilatometer cooling curve for the 25-3 alloy after solution treatment at 1200°C for 2 hours.

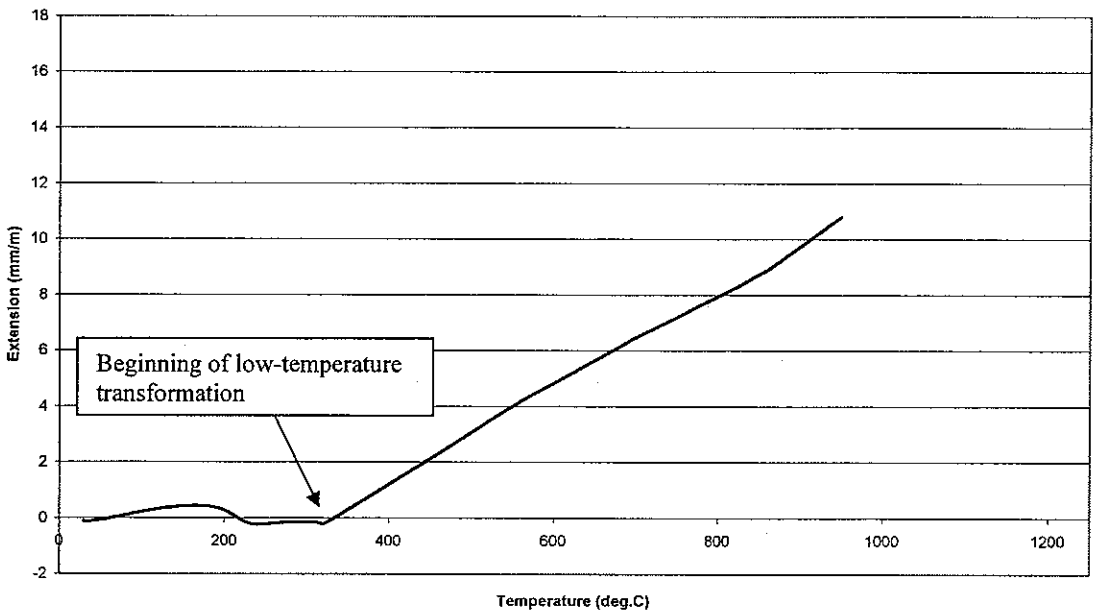


**Figure 17.** Dilatometer cooling curve for the 25-3 alloy after heat treatment at 950°C for 4 hours.

Dilatometer Results for the 25-5 Alloy

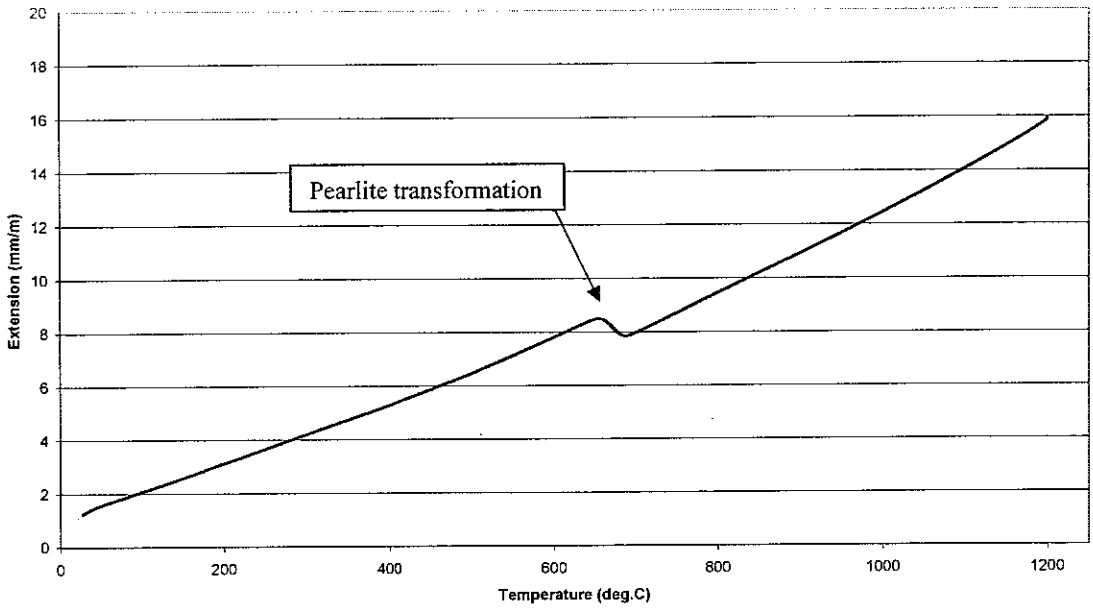


**Figure 18.** Dilatometer cooling curve for the 25-5 alloy after solution treatment at 1200°C for 2 hours.

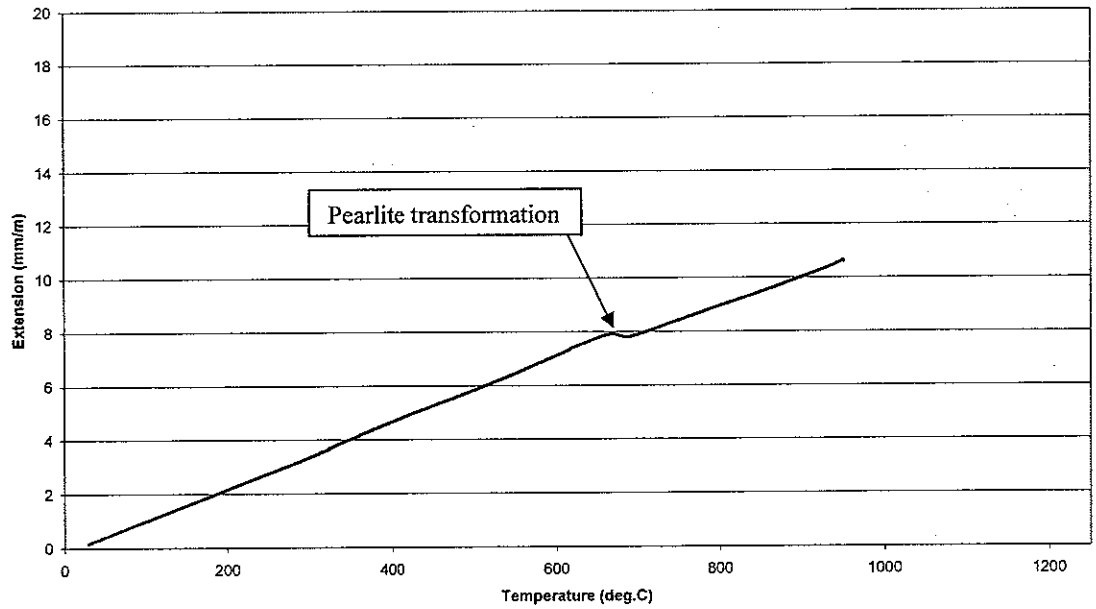


**Figure 19.** Dilatometer cooling curve for the 25-5 alloy after heat treatment at 950°C for 4 hours.

## 4. DISCUSSION

A comparison of the microstructures in the various conditions is presented below in the following sub sections.

### 4.1 As-cast microstructures

The near-eutectic 25-3 alloy exhibited eutectic carbides in a ferrous matrix consisting predominantly of austenite with a small proportion of plate-like martensite that appeared to have initiated at the carbide-austenite interface (Figure 8). The slight hypereutectic nature of this alloy was evident by a very small proportion of primary carbides. Thermal analysis results (Figure 3) and dilatometry (Figure 16) for this alloy, shows that the pearlitic transformation is suppressed upon cooling from solidification, with the resulting ferrous matrix consisting of retained austenite with partial transformation to martensite.

In contrast, thermal analysis results (Figure 5) and the dilatometer curves (Figure 18) for the 25-5 sample indicate a distinct pearlitic transformation reaction upon slow cooling. Accordingly, the as-cast structure for the hypereutectic 25-5 alloy consists of primary and eutectic carbides in a ferrous matrix that has fully transformed to pearlite (Figure 11). The presence of pearlite in abrasion-resistant white cast irons is known to have a deleterious effect on wear resistance and is therefore generally considered to be undesirable. By comparing the two alloys, it is interesting to note that the increase in carbon from 3 to 5% produces a change in the ferrous matrix from what might be considered to be a reasonably desirable structure containing martensite to an undesirable fully pearlitic structure. This may be explained by the different compositions of the ferrous matrices for the two alloys. The 25-3 is expected to contain a higher proportion of chromium than the 25-5 alloy, and the higher chromium may suppress the pearlitic reaction and enable transformation to martensite.

### 4.2 Solution treated microstructures

Both alloys exhibited slightly rounded carbides after solution treatment at elevated temperatures. Both alloys exhibited a fully austenitic ferrous matrix showing annealing twins in some areas. The main difference between the two alloys was that the 25-5 alloy was essentially free of secondary carbides (Figure 12), while secondary carbides were evident in the 25-3 alloy (Figure 9). This can be explained by the different solidus temperatures for the two alloys and that the same solution temperature of 1200°C was used for both alloys. The solution treatment temperature for the 25-3 alloy was only 39°C below the solidus and effective solution treatment was obtained. However, for the 25-5 sample, the solution treatment temperature was 65°C lower than the solidus and secondary carbides were still present at this temperature.

### 4.3 Age-hardened microstructures

In addition to the primary and eutectic carbides, both alloys exhibited secondary carbide precipitates and a high proportion of martensite in the ferrous matrix. The 25-5 alloy (Figure 13) appeared to display a higher proportion of retained austenite than the 25-3 alloy (Figure 10). This may be due to a higher carbon level in the ferrous matrix of the 25-5 alloy.

### 4.4 Thermal properties

The liquidus temperature was found to increase markedly as the carbon content increased from 3 – 5%. This is to be expected as the material becomes more hypereutectic indicating that the primary carbides begin to solidify at a higher temperature for the higher carbon alloy. This has practical implications for foundry procedures since higher pouring temperatures are required as the liquidus temperature increases.

The solidus temperature was found to decrease slightly with increasing carbon content for the alloys examined.

### 4.5 Mechanical properties

The softest state examined was the solution treated condition. This was attributed to the fully austenitic ferrous matrices in both solution treated alloys. The as-cast conditions exhibited slightly higher hardness than the solution treated condition. This could be attributed to the presence of a small amount of martensite in the 25-3 alloy and the pearlitic matrix in the 25-5 alloy. For both alloys, the age-hardened conditions displayed substantially increased hardness and this is the recommended condition for optimum wear resistance.

## 5. CONCLUSION

An understanding of the microstructures and the varying constituents in the alloy is required to obtain a better understanding of the wear and corrosion properties. The microstructure and resultant properties of high-chromium white cast irons can be controlled by varying composition and by employing various heat treatments. The current study revealed the following for high-chromium cast irons based on Fe-25Cr:

- Increasing the carbon content from 3 – 5% had a profound effect on the microstructure of the alloy. At 3% carbon, the alloy is near-eutectic and the ferrous matrix consists of austenite and martensite. In contrast, the 5% carbon alloy is predictably hypereutectic containing a significant proportion of primary $M_7C_3$ carbides. In addition, the matrix composition of the 5% carbon alloy is substantially different, transforming completely to pearlite in the as-cast condition. It is anticipated that the 5% carbon alloy possesses a ferrous matrix that is higher in carbon, but lower in chromium, than the 3% carbon alloy.

- The liquidus temperature for the alloys is very dependent on carbon content, increasing markedly with carbon content for the alloys examined.
- The solidus temperature was found to vary with carbon content. The increase in carbon content from 3 to 5% reduced the measured solidus temperature by 26°C. Similarly, results indicate that the temperature required for effective solution treatment was also found to depend on carbon content since the solidus temperature is dependent on carbon content.

SEM and EBSD techniques were found to be valuable for studying the various microstructural constituents, although some limitations of the technique do produce some difficulties, particularly when applied to age-hardened white cast irons.

Further work to be undertaken includes the following:

- Detailed microanalysis of the 25-3 and 25-5 alloys, particularly for the purpose of explaining the difference in the as-cast structures obtained for the two alloys.
- Detailed study of the kinetics of the pearlite transformation reaction.
- Detailed study of secondary carbide precipitation and decomposition to martensite by examination of microstructures at onset of transformation.
- Clarify the hexagonal close packed and possible orthorhombic nature of the crystal structure for the $M_7C_3$ carbide.
- Microhardness testing of the various microstructural constituents.

**Acknowledgements**

- Thanks to Weir Minerals Australia Ltd management for permission to publish this paper and for the use of the laboratory facilities in the Materials Services Department.
- A special thanks to the Microstructural Analysis Unit at the University of Technology, Sydney, for the use of their Electron Microscope with EBSD facilities.
- Additional thanks go to Peter Robbie [a] and Alan Hall [a] for their assistance in casting of the experimental heats, to Alan Hall [a] for manufacture of the vacuum-sealing rig and Rowan Imer [a] for performing dilatometry.

**References**

1. ASM Handbook Committee, Metals Handbook, Properties and Selections: Irons and Steels, vol. 1, American Society for Metals, Metals Park, Ohio., USA, 9th ed., 1987, 75-106.
2. Gahr, K. Z, Eldis, G. T., Abrasive wear of white cast irons, Wear, 64 (1980) 175-194
3. International Organization for Standardization (2006), Abrasion-resistant cast irons – classification (ISO 21988:2006), Geneva, Switzerland: ISO Copyright Office.
4. ASTM International (1993), Standard specification for abrasion-resistant cast irons (ASTM A532), West Conshohocken, PA, United States.
5. Frederick M. Beckett (1917), US Patent No. 1,245,552. Washington, D.C.: U.S. Patent and Trademark Office.
6. Powell, G. L. F., Morphology of eutectic $M_3C$ and $M_7C_3$ in white iron castings, Metals Forum, vol. 3, 37-46 (1980).
7. Dodd, J., Parks, J. L., Factors affecting the production and performance of thick-section high chromium-molybdenum alloy iron castings, Metals Forum, vol. 3, 3-27 (1980).
8. Tabrett, C.P., Sare, I.R., Ghomashchi, M.R., Microstructure – property relationships in high-chromium white iron alloys, International Materials Review, 1996, vol. 41, 59-82.
9. I. R. Sare, Abrasion resistance and fracture toughness of white cast irons, Met. Technol. (London), 6 (1979) 412-419.
10. Katrakova, D., Mucklich, F., Specimen preparation for electron backscatter diffraction – part I: metals, Prakt. Metallogr. 38 (2001) 10, 547-565.
11. Kogure, T. (2003). "A program to assist Kikuchi pattern analyses." Journal of the Crystallographic Society of Japan 45(6): 391-395.